Arabian Journal for Science and Engineering (2022) 47:13623–13637
https://doi.org/10.1007/s13369-022-07171-z

RESEARCH ARTICLE-CIVIL ENGINEERING

An Innovative Structural Damage Detection System for Preventive Maintenance of Wind Turbines

Muammer Ozbek[1]

Received: 23 February 2022 / Accepted: 31 July 2022 / Published online: 19 August 2022

Abstract

This study aims to develop a novel damage detection and preventive maintenance system that can be used for continuous or periodic monitoring of wind turbine components. The main features of the proposed system such as the measurement technique, data analysis procedure, and damage estimation methodology are described in detail by presenting the results of finite element model-based damage simulations, laboratory experiments, and in-field vibration tests. A hybrid measurement system with accelerometers and an automated infrared laser scanner is used to acquire vibration data with high spatial resolution. The obtained response data are then processed to extract the dynamic properties (e.g., natural vibration periods and mode shapes) of the structure. An efficient damage detection algorithm, which is based on monitoring sudden changes observed in mode shapes, is utilized to determine the location and extent of a possible damage. Within the scope of the work, a novel and simplified version of the widely used mode shape curvature method is developed for the rapid analysis and interpretation of the acquired vibration data. The applicability of the proposed methodology is demonstrated on a 61.5 m long numerical blade model proposed for NREL 5 MW Benchmark wind turbine.

Keywords Wind turbines · Structural health monitoring · Condition-based smart maintenance · Vibration measurement · System identification · Modal analysis

1 Introduction

Throughout their service lives, wind turbines are expected to resist extreme load conditions (strong winds, waves, and earthquakes) and severe environmental effects (icing, humidity, and temperature changes) [1]. Continuous vibration due to these dynamic loads may cause some fatigue cracks to be formed on structural components. If not detected at the early stages, these cracks may propagate and cause irreversible damage on the blade and the tower [2]. Therefore, the condition of these critical structures must be monitored continuously or periodically to ensure safe and reliable operation under these challenging operating conditions.

Structural health monitoring, in the simplest form, can be described as continuously observing the variation in some dynamic response characteristics, which are selected as damage indicators. Sudden changes encountered in these indicators can be related to the presence of damage. Depending on the utilized parameters, the type, location, and the degree of the damage can be determined [3, 4].

Accuracy and spatial resolution of the acquired measurements are two essential factors that affect the reliability of the analyses and the corresponding damage estimations. Depending on the type of parameters tracked (e.g., natural vibration periods [5], mode shapes [6], or wave propagation patterns [7]), it is state of the art to install accelerometers and strain gages on the structure. Indeed, these sensors are used very efficiently at locations that can easily be accessed for instrumentation and cable installation (for power supply and data transfer).

However, there may always be some points on the structure which are not accessible. A wind turbine blade is a typical example of the structural components where instrumentation is very difficult, if not impossible. Since the blade cross section gets thinner toward the tip, it is not possible to reach or place sensors to the last 20–25 m of the blade. These sensors can be placed in the blade during the manufacturing phase in

✉ Muammer Ozbek
muammer.ozbek@bilgi.edu.tr

[1] Department of Civil Engineering, Istanbul Bilgi University, Santral Campus, 34060 Istanbul, Turkey

the factory, but especially for existing turbines, it is very difficult to install dense sensor arrays and to take high-resolution measurements on the blade [8].

As a recent and innovative alternative to be used for these challenging structures, non-contact optical measurement systems, where the dynamic response is measured remotely by using the laser (Doppler Interferometry) or visible light (photogrammetry, videogrammetry, or computer vision), have been demonstrated to be very beneficial and promising. In laser interferometry, a source (laser head) continuously sends a laser beam to the target. If the object is moving, this creates a wavelength and phase difference between the sent and the received laser beams. By using the Doppler principle, the velocity or displacement of the object can be calculated with very high accuracy (in mm range) from distances up to 300–400 m [9–11].

Similarly, photogrammetry is a proven measurement method where the 3D deformation of an object can be determined by using 2D images taken from different orientations. Even though each picture provides 2D information only, very accurate 3D information related to the deformation of the structure can be acquired by synchronized processing of these images [12–15]. An extensive review and information about the use of optical measurement systems in dynamic testing of structures can be obtained in reference articles [16–18].

Within the scope of a program aiming to develop time and cost-efficient remote measurement systems (laser interferometry and photogrammetry) for structural health monitoring applications, Ozbek and Rixen [19] had successfully used laser Doppler interferometry to perform dynamic tests on a wind turbine having a diameter of 80 m. Since initial trials revealed that the intensity of the visible green/red laser beam reflecting from the blade was not sufficient to take accurate measurements, some preparations and surface treatment on the blades were required. To that end, special reflective markers had to be placed on the blade and the tower by licensed turbine climbers. Although the resulting measurements were very accurate and promising, the applicability of the method was limited due to the practical difficulties encountered in placing these markers on the structure [19].

Recently, the development of infrared (IR) Doppler vibrometers enabled this problem to be solved and made it possible to use laser interferometers for remote measurements more efficiently. Different from conventional vibrometers using visible green/red laser beam (having a wavelength of 500–680 nm), IR laser vibrometers are able to take very accurate measurements without needing any surface treatment to increase the reflectivity of the test structure. IR laser beam having a wavelength of 1500 nm is reflected by most surfaces with very high intensity. However, there still exist some drawbacks to be overcome before utilizing IR laser for health monitoring.

A visible laser has a smaller beam diameter compared with an infrared laser and can be directed by small mirrors placed inside the laser head. With the help of a computer, which controls the motion of these mirrors, the laser vibrometer can be used in scanning mode. Contrarily, IR laser having a larger beam diameter cannot be directed by reflecting or refracting the beam by small size mirrors and lenses used by conventional laser scanners. Some commercially available IR systems can take accurate measurements from large distances up to 300–400 m. However, these systems require the user to guide the laser head to the test spot manually resulting in imprecise targeting and some measurement errors. Unfortunately, there are not any operational IR vibrometers that can scan large structures from remote distances in a fast and efficient manner.

Within the scope of this project, a new guidance and control technique was developed. As can be seen in Fig. 1, the laser source was mounted on a motorized platform that can rotate about horizontal and vertical axes simultaneously. The laser was aimed at the target simply by rotating the platform instead of guiding the beam by optical methods. The technical details related to the implementation of this system as an automated laser scanner are described in more detail in [20]. For convenience, this work will also very briefly review the accuracy of the measurements acquired by using this new scanner and how it can be utilized as an integrated module of a health monitoring system.

As can be seen in the figure, an integrated camera system enables the user to monitor the structure continuously through a computer screen. By selecting some points on the screen, the user can easily define several measurement paths or grid-like patterns. The number of test points and the corresponding spatial resolution can easily be increased by dividing these selected patterns into the desired number of segments. A specialized software program determines the coordinates of these points, while the laser beam is directed to these target points automatically. The successive measurements taken in scanning mode can be seen in Fig. 2. Since IR measurement cannot be seen by the naked eye, a visible red laser is used to validate the accuracy of the targeting system. Laser measurement is also synchronized with the response data acquired by the accelerometer(s) installed on the structure. Considering the fact that excitation levels may change during the experiment, accelerometer data are used as a reference to scale and combine laser measurements taken at different times.

2 Testing Targeting Precision and Scanning Efficiency Through Outdoor Experiments

Figure 3 shows the experimental setup used for the outdoor feasibility tests. These tests were performed to check whether

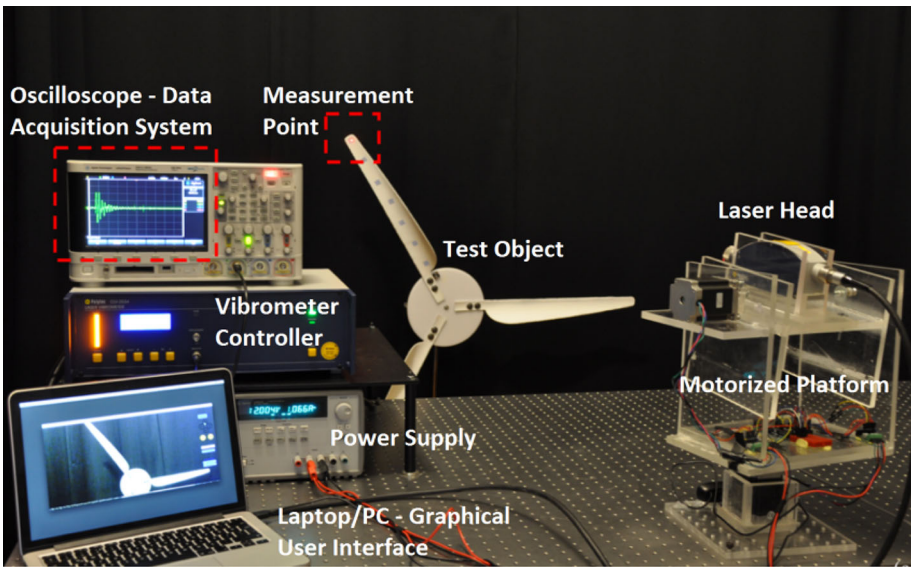

Fig. 1 The motorized platform developed for the laser scanner [20]

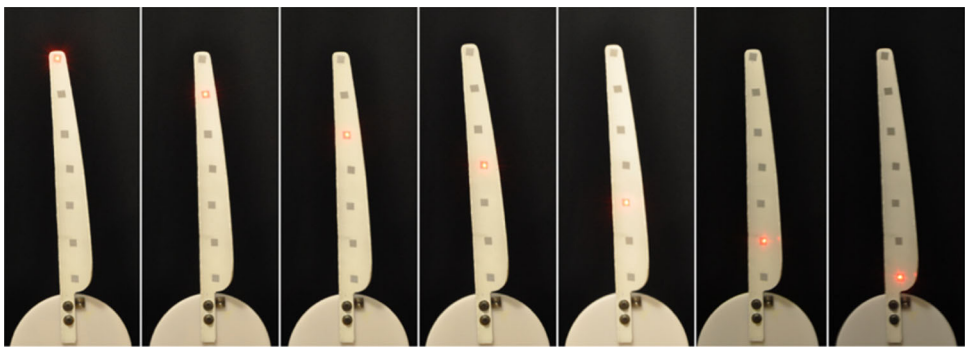

Fig. 2 Scanning of successive measurement points

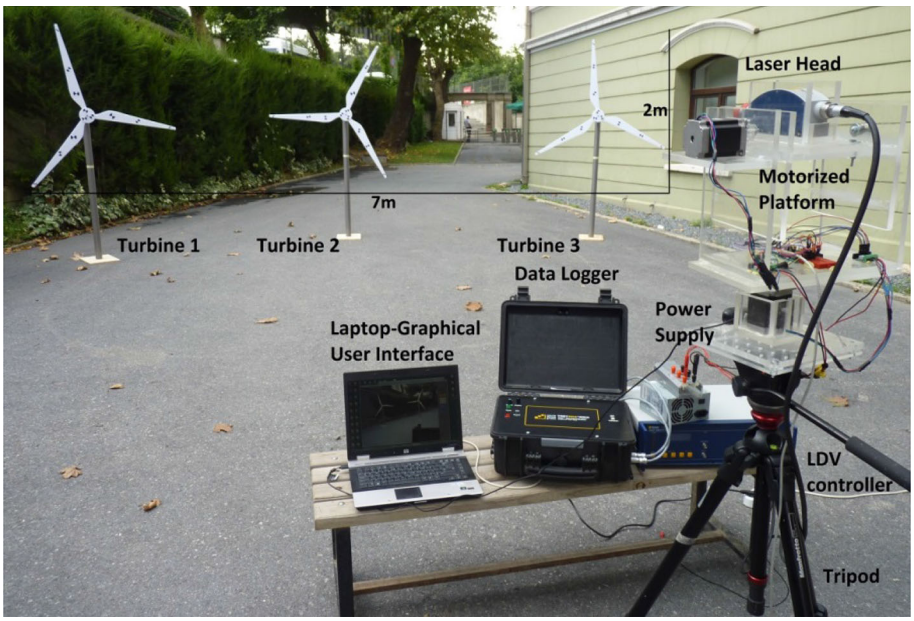

Fig. 3 The test setup used for the outdoor measurements [20]

the designed system is able to scan complex geometries in a fast and efficient manner. Depending on the required spatial resolution, all three turbine models shown in the figure could be scanned within a short period of 10–15 min. In order to see how the error was accumulated after scanning several measurement points, the laser vibrometer was programmed to return to the first target after all the points on the three turbines were measured successively. The laser spot, which returned to the initial position, was observed to be very close to its starting point. The deviation between the coordinates of the initial and final points was in the range of 3–4 mm at maximum.

The ratio of the maximum deviation (4 mm) to the horizontal dimension of the field of view (approximately 7 m) was used to calculate what the error would be, if the same targeting system was utilized to scan large commercial wind turbines. It is expected that the same targeting precision can be reached in scanning large structures as well. Regarding the abovementioned tests conducted by Ozbek and Rixen [19] on the 80-m diameter turbine, the corresponding error is calculated to be in the range of $\pm$ 5 cm. It is worth mentioning that this value does not represent the error made in targeting a single point directly. It is the accumulated error when the system scans several points on a large structure and then returns to the initial point. As mentioned earlier, more detailed information related to calibration of the system, the measurement accuracy, and the results of the indoor/outdoor feasibility tests can be reached through the article [20] which focuses on the guidance system specifically.

The data acquired through outdoor vibration experiments are also used for the identification of possible damage on the blade. The results of these analyses will be discussed after the main features of the proposed methodology are introduced. Initially, the mathematical accuracy of the utilized algorithm and the reliability of the corresponding damage estimations are demonstrated on FE models. Working on a FE model makes it possible to control all analysis variables (e.g., damage level) very accurately and eliminates other possible sources of uncertainty and practical difficulties related to the measurements.

3 Data Processing and Analysis Methodology

The damage detection algorithm utilized in this work is mainly based on comparing the mode shapes of the healthy reference and the damaged structure. The methodology does not require using a FE model to determine the location of the damage. The flawed segments can always be identified very accurately by just comparing the modes of the healthy and damaged components. However, some supplementary calculations should be performed on a FE model to interpret what these shape changes correspond to.

Using a representative FE model always enables complicated damage patterns to be visualized and understood clearly [21]. Model-based damage detection applications make it possible to determine the location and degree of the damage on the components with complex geometries or deformation characteristics [22, 23]. FE modeling has become a standard procedure in designing contemporary engineering structures. Therefore, without any extra investment, it is possible to utilize damage detection methods, which can be applied to already existing FE models, as a reasonable and cost-efficient approach. Such an approach enables to analyze complicated damage scenarios, which involve simultaneous damage at multiple locations, beforehand [24, 25]. Obtained results can be stored in a database and used to monitor the health condition of the structure regularly or after extreme events such as earthquakes or hurricanes.

The dynamic analysis procedure proposed in this work is based on the well-known mode shape curvature method. Although both algorithms involve the comparison of the mode shapes extracted from the healthy and the damaged structures, these shapes are processed differently. In conventional mode shape curvature method, the damaged mode shape is subtracted from the healthy reference. Then, this difference is processed by several algorithms to compute damage indices. Damage indices are the key parameters which show the location of possible flaw(s). If the degree of the damage is also of concern, some scale factors should be derived to use these damage indices for estimating the extent of the flaw. In the proposed method, however, the healthy and the damaged modes are processed simultaneously and the stiffness loss is detected directly by computing the angles between the modes. The FE model enables to relate the calculated angles to the damage level in an easier and more accurate way. The main focus of this study is demonstrating whether the proposed method can be used as an efficient health monitoring system for wind turbine components such as the blades and the tower. More detailed information on the mathematical background and the derivation of the technique can be reached through the references [26, 27]. This work also proposes a novel and simplified analysis algorithm, which is very efficient, accurate, and easy to implement on the existing finite element models.

If damage occurs on a structural component, it affects the dynamic parameters (vibration periods, damping ratios, and mode shapes) of the system [5, 6]. The deviation in natural periods is an important indicator of possible damage, but its location and extent can only be determined by monitoring the corresponding variation in mode shapes [28]. Below, the effect of the damage on the mode shape is described by presenting the results of the analyses performed on a 10 DOF (degrees of freedom) system shown in Fig. 4. The model displayed in the figure can be used to represent both the tower and the blade. For simplicity, the considered system consists

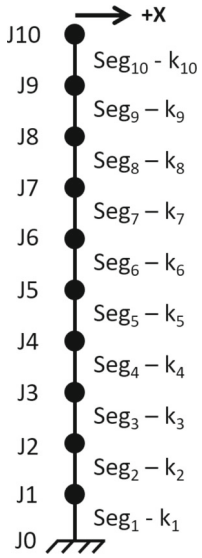

Fig. 4 The 10 DOF system analyzed

of 10 lumped joint masses, which can vibrate in one direction only. In the figure, the symbol J stands for the joint. Joint 0 can be considered as either tower-foundation or blade-hub connection. Similarly, the Seg_i and k_i correspond to the ith segment of the blade (or the tower) and its stiffness, respectively.

Figure 5a, b shows how the first mode of this system changes depending on the location of the damage. In the figure, horizontal and vertical axes show the modal amplitude and the joint (node) number, respectively. In both Fig. 5a, b, the blue curves represent the first mode of the undamaged reference. Similarly, red curves show the modes calculated for the flawed structure. Modes are dimensionless shape functions which are in fact the orthogonal vectors obtained from eigenvalue analysis. In the figure, the reference healthy structure is compared with a case where the selected component loses 90% of its initial stiffness. Such an extreme damage is considered just for showing the variation in the mode more clearly. In Fig. 5a, only the structural member between Joint 1 and Joint 2 (e.g., the second blade segment) is damaged. In Fig. 5b, however, the damage is only at the member between Joint 5 and Joint 6 (e.g., the sixth segment). The damaged member is also displayed by red color on the vertical axis.

The figure clearly reveals that the relative modal displacement—the difference between the modal amplitudes calculated for successive joints—is significantly higher at the damaged element. In Fig. 5a, where the second segment is damaged, Joint 2 is displaced considerably more compared to Joint 1. In the same way, in Fig. 5b, where the flaw is localized at the sixth segment, Joint 6 is obviously displaced more with respect to Joint 5. In this work, a new methodology is presented to quantify and interpret this observed variation.

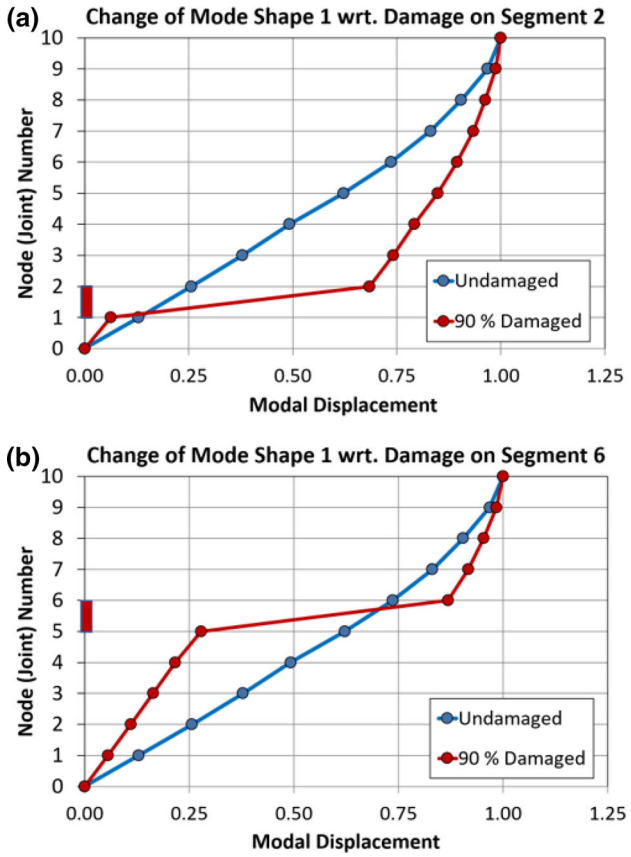

Fig. 5 Change of the first vibration mode depending on the damage location

As mentioned before, the mode shape calculated for the healthy structure is used as a reference. The modal displacements of the damaged structure are then compared with these reference values. The notation used for the modal displacements is shown in Fig. 6. In the figure, $\phi_{i,1,h}$ shows the modal amplitude calculated at joint number i for mode number 1. The symbols h and d, which are used as the third indices, represent the healthy and the damaged states, respectively.

As shown in Eq. (1), a new chart, which will be called as *Mode Shape Angle Diagram*, can be obtained by picking data points with coordinates $(x_i\ ;\ y_i)$ where x and y coordinates are the modal displacements of the ith joint calculated for the healthy and damaged structures, respectively.

$$(x_i\ ;\ \ y_i) = (\phi_{i,1,h}\ ;\ \ \phi_{i,1,d}) \tag{1}$$

Following the analyses conducted on the healthy structure, successive simulations are performed by creating damage on some pre-determined component(s). A possible damage on the element can be represented by reducing its stiffness gradually. As shown in Eq. (2), the stiffness *"k"* (kN/m) of

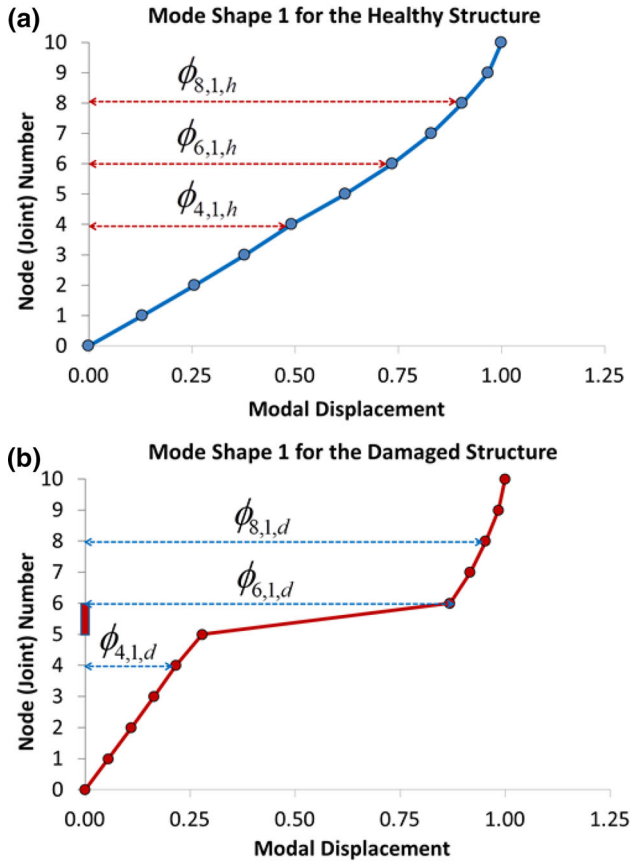

Fig. 6 The notation used for modal displacements

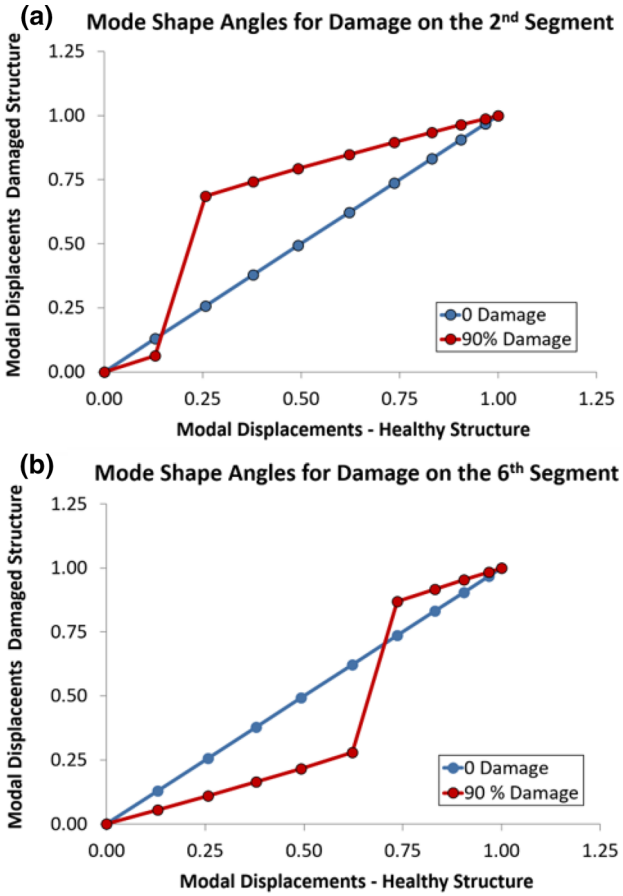

Fig. 7 Mode shape angle diagrams drawn for several damage scenarios

a structural component is directly proportional to the modulus of elasticity of the material used *"E"* (kN/m^2) and the moment of inertia "*I*" (m^4) of the cross section. The extent of the damage can be controlled simply by adjusting the material properties, more specifically, the modulus of elasticity value. In Eq. (2), "*L*" is the height or length of the member which does not change depending on the damage.

$$k \propto \frac{E\,I}{L^3} \tag{2}$$

The damage on the selected component is then gradually increased and the corresponding effect on the modal parameters is calculated by performing successive eigenvalue analyses. The mode shapes calculated for different damage levels are stored in a database for further operations. Damage level, i.e., % stiffness loss of the element, can be calculated by using Eq. (3).

$$\%\ \text{Damage} = \left(1 - \frac{\text{Stiffness of the damaged member}}{\text{Stiffness of the healthy member}}\right) \times 100 \tag{3}$$

The healthy reference can be considered as a damaged structure with 0% damage level. Therefore, the abovementioned *Mode Shape Angle Diagram* can also be drawn for the healthy structure. Since for all the joints, $\phi_{i,1,h} = \phi_{i,1,d}$, x and y coordinate values would be the same and the resulting diagram would correspond to $y = x$ graph, which forms a 45° angle with the horizontal axis. The *Mode Shape Angle Diagrams* drawn for the damage cases in Fig. 5a, b (90% damage at the second and sixth members) are presented in Fig. 7a, b.

As can be seen in Fig. 7a, where the second segment on the blade is damaged, the slope of the line segments suddenly changes at the bottom and top joints of the damaged member, namely at Joint 1 and 2. Similarly, when the sixth segment is damaged, the slope suddenly changes at the bottom and top joints of the sixth segment only (Joint 5 and 6). However, in both figures, the slopes of the segments do not change at the joints of the undamaged elements. For example, in Fig. 7b, the slope is the same for the first five line segments. Some reference curves can be obtained by calculating how the slope and the angle change at the joints as a function of the damage level.

The angle notation used in this work is presented in Fig. 8.

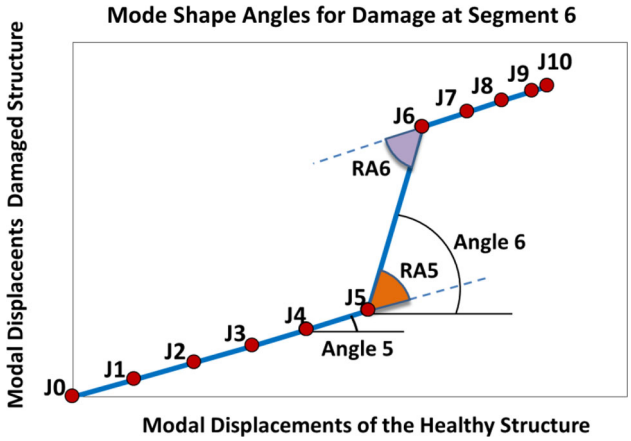

Fig. 8 Angle Notation used in the analyses

There can be seen 11 joints (J0 is the base joint) and 10 different segments in the figure. The angle between each segment and the horizontal x-axis is calculated separately. $Angle_i$ is the angle between the ith segment and x-axis. This angle can be calculated by Eq. (4). Similarly, the symbol RA_i stands for $Relative\ Angle_i$. As shown in Eq. (5), RA_i is the difference between the angles calculated for stories $i + 1$ and i.

$$Angle_i = \text{atan}\left(\frac{\phi_{i+1,1,d} - \phi_{i,1,d}}{\phi_{i+1,1,h} - \phi_{i,1,h}}\right) \tag{4}$$

$$RA_i = Angle_{i+1} - Angle_i \tag{5}$$

If the $(i + 1)$th member is undamaged, RA_i is approximately equal to zero. However, RA_i increases considerably depending on the damage level. Damage simulations performed on the FE model clearly indicate how *Relative Angle* RA_i changes depending on the % stiffness loss. During the analyses, the stiffness of the flawed component is reduced gradually, mode shapes are extracted and the corresponding Relative Angles are calculated at each step. The Relative Angles obtained for different damage levels are then used to generate *Reference Damage Curves*.

Figure 9a shows several *Mode Shape Angle Diagrams* drawn for *Relative Angle 5* which is the damage indicator for the sixth blade segment. The diagrams are obtained for stiffness losses varying between 0 and 90%. Similarly, Fig. 9b presents the *Reference Damage Curve* which displays the variation in *Relative Angle 5* depending on the % damage. In Fig. 9b, the horizontal and vertical axes represent % stiffness loss and the corresponding Relative Angle (in degrees), respectively. Reference curves calculated for different blade segments may change depending on the physical properties of the section, more specifically, on the overall mass and stiffness distribution. Therefore, they should be calculated

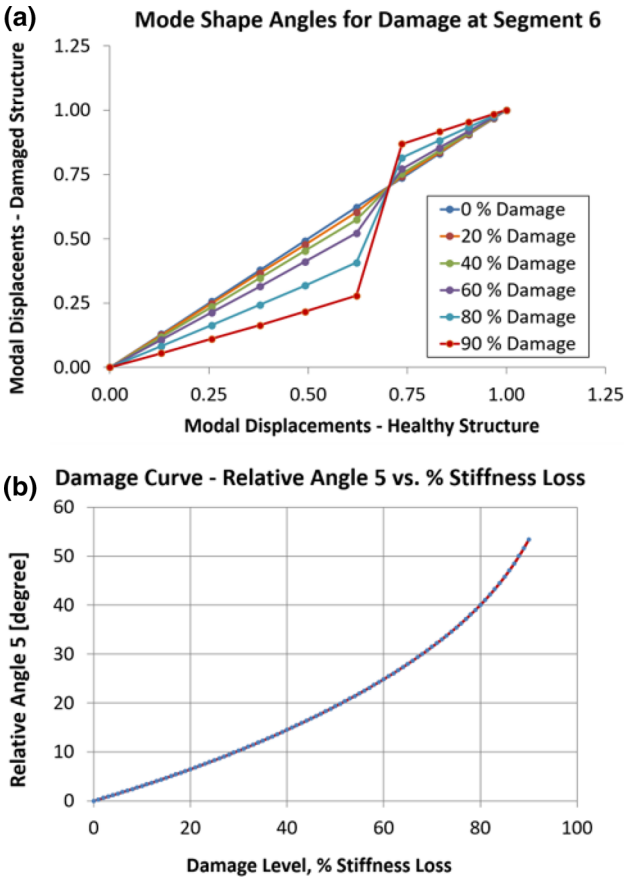

Fig. 9 **a** Mode shape angle diagram calculated for the case segment 6 is damaged. **b** Reference damage curve for Relative Angle 5

separately. It should be noted that to draw Fig. 9b, all damage cases between 0 and 90% stiffness losses are analyzed by reducing the stiffness by 1% at each step. Hence, Fig. 9b has in fact a higher resolution and includes more data points (90 points) compared to Fig. 9a which displays some selected damage levels only.

The most important difference between the conventional mode shape curvature method and the algorithm proposed in this work is that *Reference Damage Curves* are needed to determine which damage level the observed relative angles correspond to. Therefore, it is required to perform successive damage simulations on a validated FE model of the structure. Since FE modeling is a standard procedure in designing almost all contemporary engineering structures, it is assumed that these models exist and are readily accessible to be used for damage detection purposes. The advantage of the method is that it is very efficient, accurate, and easy to implement on the existing models. It also enables complicated damage patterns to be visualized and understood clearly.

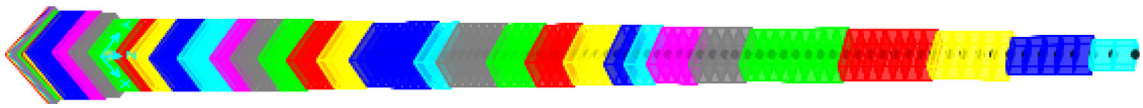

Fig. 10 SAP2000 representative blade model

4 Damage Simulations on Wind Turbine Blade Model

The mathematical accuracy of the utilized technique is initially tested on a FE model to eliminate possible sources of uncertainty related to the measurements. The efficiency of the damage detection algorithm is demonstrated on the numerical blade model of the 5 MW NREL wind turbine having a diameter of 126 m. In order to develop an open-source Benchmark model, the structural properties of the 61.5 m long blade are shared freely by Sandia National Laboratories [29]. The available technical data (e.g., the mass density, moment of inertia, and stiffness values) are used to generate a representative SAP2000 (Structural Analysis Program) model which is shown in Fig. 10.

The proposed methodology can currently be applied to the turbines which are at park condition. Extending this technique to the analysis of rotating components is at the center of our ongoing research studies. It should be noted that once the rotor starts rotating, its dynamic properties (frequencies, damping ratios, and mode shapes) change significantly depending on the rotational speed. The variation in these aero-elastic parameters cannot be determined accurately by ordinary finite element tools. Therefore, a special software FAST (Fatigue, Aerodynamics, Structures, and Turbulence), which was developed for dynamic analysis of rotating turbines specifically, will be used for this purpose. Using such an aero-elastic simulator will make it possible to estimate the variation in the mode shapes of the healthy reference turbine due to changing wind and rotor speed. Then, the dynamic response of a turbine with a damaged blade will be analyzed by FAST for the same operational conditions. In this way, it is aimed to distinguish between the response variations due to damage and rotational speed. The 5 MW NREL wind turbine model is already integrated into the FAST simulator. Hence, demonstrating the capabilities of the method on this Benchmark model is an essential step for future analyses.

In Fig. 10, different colors are used to represent the segments with different cross-sectional properties. The blade model is 61.5 m long and consists of 37 segments in total. To increase the accuracy of the analysis, each segment is also divided into smaller elements with a maximum length of 500 mm. As can be seen in the figure, blade segments have rectangular cross sections. Since the model is not used for aerodynamic simulations but structural analysis and damage detection, the shape of the sections does not affect the results.

Table 1 The comparison of eigenfrequencies for model validation

Structural mode	SAP2000 [Hz]	NREL model [Hz]
First Flapwise bending (out of rotor plane)	0.87	0.87
First Edgewise bending (in rotor plane)	1.07	1.06
Second Flapwise bending	2.61	2.68
Second Edgewise bending	3.91	3.91
Third Flapwise bending	5.84	5.57

Once the model is generated, the dynamic parameters obtained from SAP2000 analyses are compared with the reference values reported in [29]. Table 1 summarizes the eigenfrequencies specified for the NREL Benchmark model and those obtained from the SAP2000 model. As can be seen, the frequencies calculated for the first five vibration modes are very close to the reference values, validating that the SAP2000 model can be used to represent the structural behavior of the blade accurately.

The validated model is then used to perform damage simulations at different locations on the blade. Reference damage curves are obtained by changing the stiffness of only one segment at a time. For this purpose, the stiffness of the analyzed segment is reduced by 1% at each step by adjusting the modulus of elasticity value, and then, the corresponding mode shape is calculated. For the selected segment, all damage levels varying between 1 and 75% stiffness losses are simulated successively. The abovementioned mode shape angle method is used to develop a database showing how relative angles change as a function of the damage condition of the blade.

The analyses are initially conducted for four different segments (A-B-C-D) on the blade, and the corresponding angle variations are displayed in Fig. 11. The segments A, B, C and D are 26.6, 34.9, 43.1 and 51.3 m away from the root region of the blade, respectively. In the figure, Relative Angle 58 is the damage indicator for Segment A. Similarly, the damage on Segments B, C, and D are represented by Relative Angles 74,

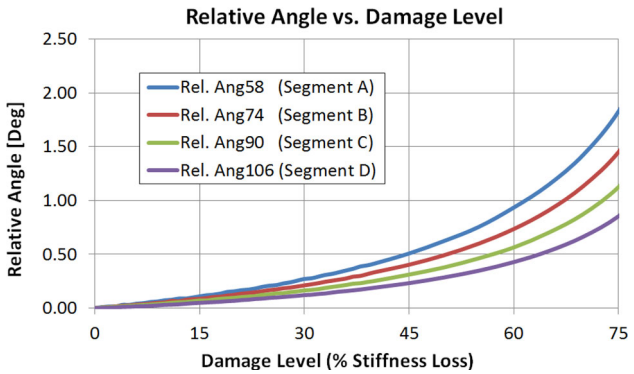

Fig. 11 Reference damage curves for Segments A, B, C, and D

90, and 106, respectively. It should be noted that the curves shown in Fig. 11 are calculated by simulating damage at one segment at a time. For example, for monitoring the change in Relative Angle 58 with respect to damage level (the blue curve), it is assumed that there is damage at Segment A only and that other segments B, C, and D are intact. These curves are then used as *Reference Damage Curves* for evaluating the results of further analyses and simulations.

In order to validate that the Relative Angle calculated for a blade segment does only change depending on the health condition of this particular segment and is not affected by the damage that happens at other locations, the variation in the abovementioned Relative Angles is monitored during simultaneous multiple damage simulations. The results of these analyses are presented in Fig. 12.

Figure 12a shows how Relative Angle 58, which is the damage indicator for Segment A, changes in several analyses. As can be seen in the figure, the curves calculated for different damage cases overlap almost completely. Relative Angle 58 calculated for a case, where there is damage at Segment A only, is almost the same as the Relative Angle 58 calculated for a case, where there is simultaneous damage at Segments A–B–C–D. Similarly, in Fig. 12b, it can be seen that Relative Angle 74 is dependent on the health condition of Segment B only. Even if Segments A, C, and D are damaged simultaneously as well, they do not affect Relative Angle 74. The same tendency can also be seen in Fig. 12c, d.

Once it is demonstrated that the proposed mode shape angle method allows linear superposition of damage levels calculated for different segments, a more complicated scenario involving simultaneous damage at multiple blade segments is analyzed. As a validation test, a case where all four elements (A–B–C–D) are damaged simultaneously is simulated. For this purpose, modulus of elasticity values of the segments A, B, C, and D is reduced to represent damage levels varying between 20 and 35% stiffness losses. The mode shape of the damaged structure is extracted and compared with the reference healthy state to calculate Relative Angles.

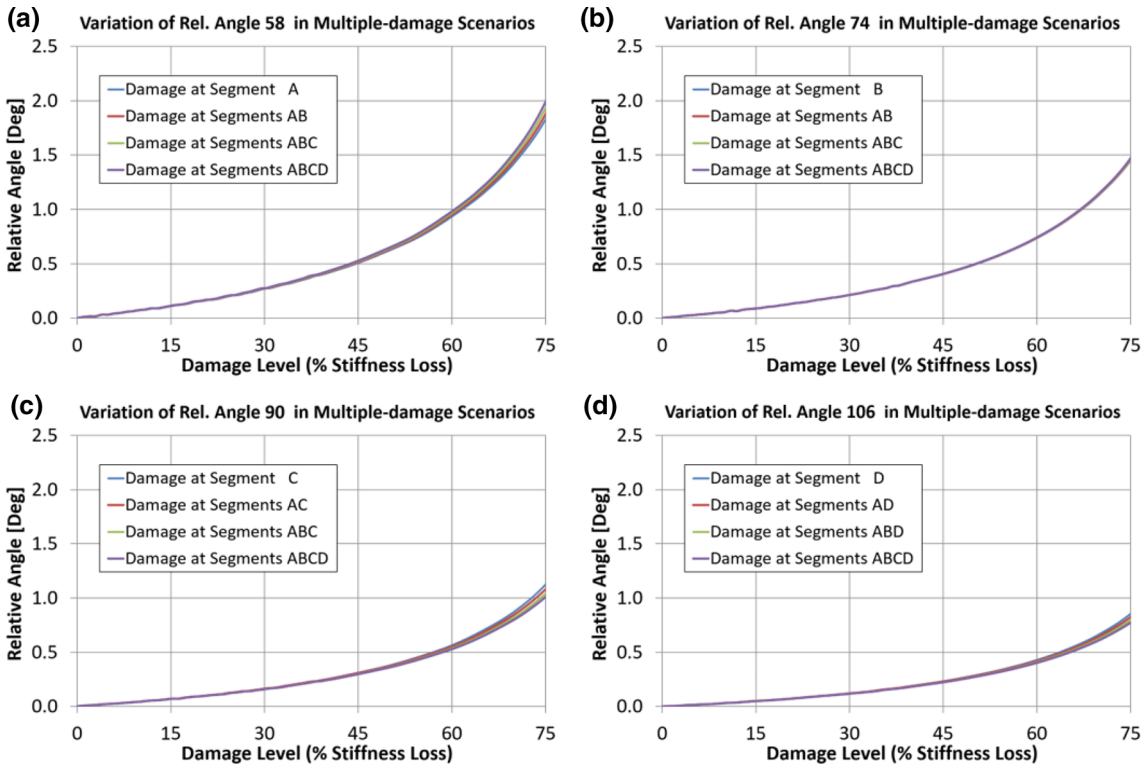

Fig. 12 Change of relative angles in several multi-damage simulations

Table 2 Reference damage levels (single damage at a time) used for the validation test

Damage level (% stiffness loss)	Rel. Ang58 (Segment A)	Rel. Ang74 (Segment B)	Rel. Ang90 (Segment C)	Rel. Ang106 (Segment D)
20	*0.157	0.124	0.096	0.069
21	*0.167	0.135	0.103	0.075
22	0.173	0.141	0.108	0.079
23	0.183	0.148	0.112	0.086
24	0.199	0.158	*0.124	0.089
25	0.209	0.168	*0.129	0.096
26	0.214	0.175	0.138	0.099
27	0.230	0.185	0.140	0.105
28	0.240	0.192	0.149	0.110
29	0.256	0.202	0.156	0.115
30	0.272	*0.212	0.165	0.122
31	0.277	*0.222	0.170	0.125
32	0.293	0.232	0.177	0.132
33	0.309	0.246	0.188	0.137
34	0.319	0.256	0.197	*0.146
35	0.335	0.266	0.207	*0.154

Table 3 Comparison of simulated and estimated damage for multi-damage scenario (simultaneous damage at segments A, B, C, and D)

Element	Distance to the root [m]	Simulated damage %	Damage indicator	Calculated angle [Deg]	Estimated damage %	Estimation error (%)
A	26.6	20	Rel Ang 58	0.161	20.4	2.0
B	34.9	30	Rel Ang 74	0.213	30.1	0.3
C	43.1	25	Rel Ang 90	0.126	24.3	2.8
D	51.3	35	Rel Ang 106	0.147	34.1	2.6

Table 2 shows the % stiffness losses and the corresponding Relative Angles, which are displayed in Fig. 11, in more detail. The values presented in Table 2 are obtained from single damage analyses and will be used as a reference for the multiple damage validation test described below. For simplicity, only the damage range considered in the validation test, namely the values between 20 and 35%, is displayed in the table. Similarly, the relative angles calculated for the multiple damage validation test are summarized in Table 3. By using linear interpolation of the reference values shown in Table 2, the damage at Elements A, B, C, and D are estimated. The Relative Angle values used for the interpolation are marked with the * symbol in the table.

As can be seen in Table 3, stiffness losses can be calculated with very high accuracy even for complicated simulations involving simultaneous damage at four different locations on the blade. In the table, the term "simulated damage" refers to the stiffness loss assigned to some predetermined elements on the SAP2000 model. Since generated on the numerical model, the exact value and the location are known very accurately. Estimated damage, however, is obtained by reverse calculation or more specifically, the dynamic analyses of the vibration response acquired on the structure. As shown in the table, the maximum estimation error is 2.8% which can be considered to be very promising. The same values are also presented in graphical format in Fig. 13.

5 Dynamic Tests and Damage Analyses on the Blade and the Scaled Turbine Model

This section aims at discussing whether the location and the degree of the damage on a structural component can be determined through laboratory experiments and outdoor vibration measurements. For this purpose, before starting the outdoor

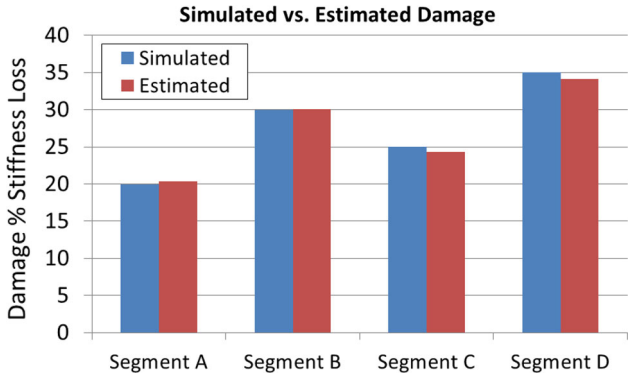

Fig. 13 Comparison of Simulated and Estimated Damage for Multi-damage scenario

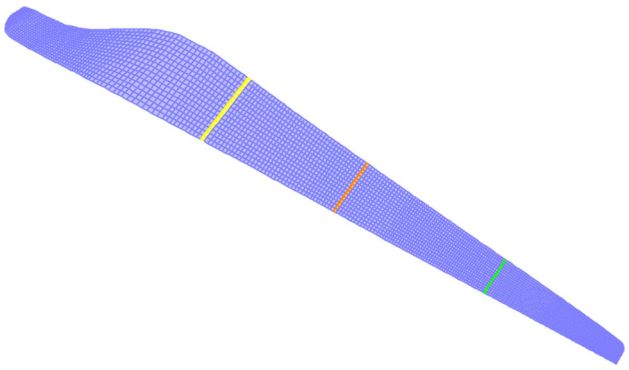

Fig. 15 Damaged blade segments (SAP 2000 model)

tests shown in Fig. 3, first, a turbine blade is tested in the laboratory as a single component. Testing the component under controllable boundary conditions enables FE models to be used in estimating the damage level. In order to simulate the boundary conditions selected in the FE model, the root of the blade is firmly fixed by a press. Vibration measurements are taken on the healthy component, and the mode shapes shown in Fig. 14 are extracted.

Following the tests performed on the healthy reference, the blade is physically damaged by cutting the pre-determined sections with a saw. The most important drawback related to this operation is the quantification of the flaw made on the element. Therefore, some supplementary static tests are decided to be performed to validate the degree of the damage on the tested component.

As demonstrated in Fig. 15, the blade is divided into 240 sections and the segments 60 (yellow), 100 (orange) and, 160 (green) are damaged both on the FE model and on the real blade. First, segment 60 is damaged by cutting. In order to quantify the flaw made on the blade, a single point mass is attached to the tip and the corresponding static tip deformation is measured by a laser distance meter. Then, by adjusting section properties (e.g., modulus of elasticity) in the SAP2000 program, the stiffness of segment 60 is reduced gradually until the same tip deformation value is also obtained from the FE model. In other words, the reduction in the stiffness of segment 60 is determined by reverse calculation by using measured static deformation.

The same approach is applied step by step to calculate the degree of the damage at other sections. Similarly, segment 100 is damaged, the aforementioned static tests are performed and the corresponding tip deformation is measured. However, in this case, the obtained tip deformation is due to the combined effect of the damage at Segments 60 and 100. Since the stiffness loss in segment 60 is already calculated, the damage at Segment 100 can be obtained by changing only the properties of Segment 100 in SAP2000.

As the third step, Segment 160 is cut and the abovementioned static test procedure is repeated. The deformation obtained from the third static test is caused by the simultaneous damage at Segments 60, 100, and 160. Since the stiffness losses at segments 60 and 100 are known previously, the damage at segment 160 can be estimated by fine-tuning the section properties of Segment 160 only on the FE model.

Fig. 14 Mode Shapes calculated for the healthy reference blade

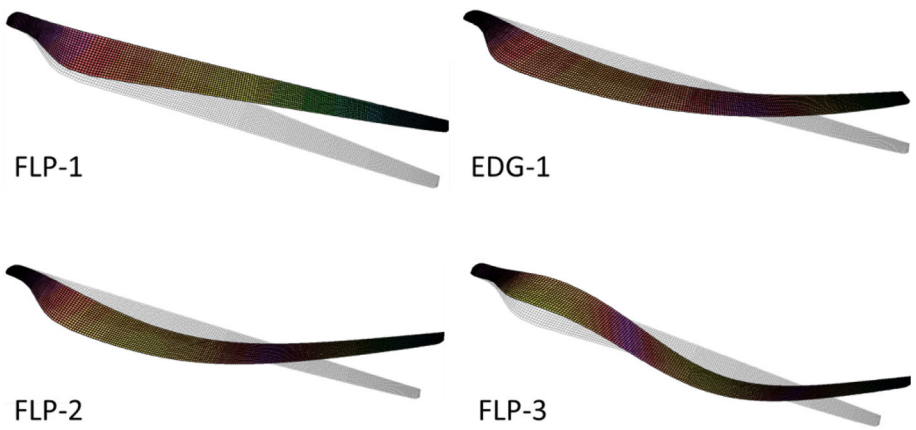

Table 4 Comparison of Theoretically and Experimentally Calculated Damage Levels

Element	% Damage static test	% Damage dynamic test	Error dynamic versus static
Seg 60	38.2	41.0	7.4%
Seg 100	51.4	56.3	9.6%
Seg 160	62.5	69.4	11.1%

Once the static tests are completed, dynamic parameters of the damaged blade are extracted through vibration measurements. The mode shape of the blade, which is damaged at three different segments simultaneously, is calculated and compared by the mode of the reference healthy blade. As mentioned before, a reference accelerometer signal is necessary to scale and then combine the laser measurements taken at different times and locations. It should be noted that during the static tests, the accelerometer [30] was already placed on the blade. Table 4 summarizes the corresponding damage estimations.

As can be seen in the table, the damage levels estimated by static and dynamic tests are very close. The estimation error is proportional to the damage level and has a maximum value of 11.1%. The observed difference can be attributed to both static and dynamic tests. As mentioned before, calculation of the damage by static tests is based on a step-by-step procedure. First, the damage at Segment 60 is calculated by using the results of first static test. Then, the residual stiffness value calculated for Segment 60 and the results of the second static test are together used to estimate the damage at Segment 100. Finally, the values obtained for Segment 60 and 100 are both used with the results of the third static test to estimate the damage at Segment 160. Such an approach may result in a propagating systematic error. The uncertainty related to Segment 60 affects the other results directly. This tendency can be seen in the table. The error calculated for one segment is always greater than the error obtained for the previous ones, i.e., $err_{Seg160} > err_{Seg100} > err_{Seg60}$.

When the theoretical results presented in Table 3 are compared with the experimental results shown in Table 4, it can be seen that the estimation error obtained from the experimental analyses is larger. While the max. error in Table 3 is 2.8%, it is 11.1% in Table 4. As described below, a major part of the experimentally calculated estimation error is attributed to the practical difficulties in the quantification of the flaw made on the blade or similar practical limitations related to the experiment.

A part of the error can also be related to the mathematical uncertainty related to the method. As can be seen in Fig. 14, for high damage levels (65–70%), there happens some scatter between the relative angles calculated for single damage and multiple damage scenarios resulting in some decrease in accuracy. In Table 3, the maximum damage is 35%. However, Table 4 includes the cases where damage changes between 41 and 69.4%. Damage levels of 40% or higher may not be reasonable in practice. Most probably, a possible damage (e.g., crack) will be detected much earlier before it reaches such a critical state and causes 40% stiffness loss. Therefore, it can be concluded that the damage levels considered (20–35% loss) in Table 3 are more reasonable. It is expected that the estimation error would be in the range of 5–6% in practical applications. Even an 11.1% error, which corresponds to an extreme case of 69.4% stiffness loss, is a very satisfactory and promising result to implement this method for the structural health monitoring of large wind turbines.

Following the component tests, the damaged blade is mounted to the rotor to be used for the outdoor tests. Vibration measurements are taken on two different blades on the turbine, namely the healthy reference and the damaged blade. These two blades are supposed to be identical in terms of material properties, geometry, and boundary conditions, so the mode shape extracted for the healthy blade is expected to be used as a reference for the damaged one. The above-mentioned dynamic test and measurement procedure is repeated and the corresponding modal properties are calculated. Damage parameters are identified by comparing the mode shapes obtained for the flawed and the healthy blade.

As previously mentioned, the methodology proposed in this work does not require using a FE model to determine the location of the damage. The damaged segments can always be identified very accurately by just comparing the modes of the healthy and damaged components. However, some supplementary calculations should be performed on a FE model to understand what the observed shape changes correspond to.

Unfortunately, it is not possible to accurately determine the stiffness values of blade-rotor, nacelle-tower, and tower-foundation connections for the scaled wind turbine model shown in Fig. 3. Since a FE model, which shows all the components (e.g., blade, rotor, and tower) together as a whole system, is not available, the outdoor measurements are only used to determine the location of the damage. For future studies, using a validated FAST model is expected to overcome this drawback and make it possible to apply the proposed method for dynamic testing of full-scale wind turbines more efficiently. There is no need for a FE model for damage localization purposes. However, in calculating the extent of the damage, where FAST models will be needed, the reliability of the method will depend on how accurate those models represent the real turbines.

By using the vibration data acquired through outdoor dynamic tests, the condition of the flawed component is analyzed. Figure 16 shows the damage locations estimated for

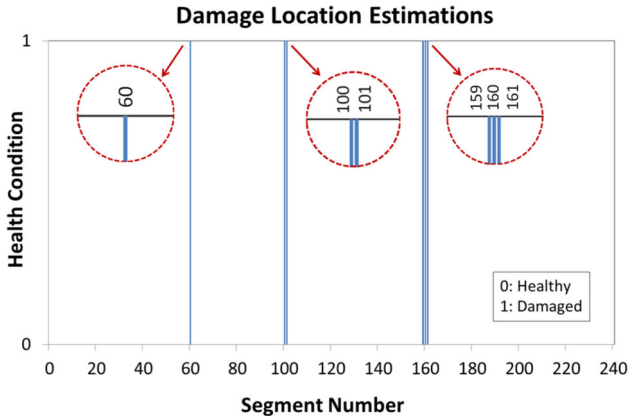

Fig. 16 Damage location estimates for the blade of the scaled turbine model

the monitored blade. The figure clearly reveals that by comparing the modal parameters obtained through experiments only, the location of the damage can be determined with very high accuracy. In Fig. 16, the horizontal and vertical axes represent the segment ID number and damage state, respectively. Since a complete FE model is not available, it is not possible to quantify the damage. Therefore, there are only two states to define the current condition of a blade segment, namely the healthy and damaged states. If the relative angle calculated for a segment is zero, it is considered to be healthy. A change observed in the angle indicates that the component is damaged.

As can be seen in Fig. 16, the method can successfully detect which segments are damaged (60, 100, and 160). However, for segment 100, the algorithm estimates that the neighboring segment 101 is also damaged. Similarly, for segment 160, the results indicate some damage at nearby segments 159 and 161. This error can be attributed to two possible reasons. As one of the reasons, the healthy blade used as a reference may not be exactly representing the healthy state of the damaged blade. Even if they are considered to be identical, some very slight differences may exist, which can affect the results. Secondly, the error can also be considered as a side effect of having a very high spatial resolution. In this study, the blade is divided into 240 cells in the longitudinal direction and the average length of the sections is in the range of 5 mm. Even if the laser always targets the same location in space throughout the measurement, during vibration, different segments may cross over the laser spot. Since the vibration amplitude is directly proportional to the distance from the root (rotor hub), the problem becomes more evident as the point gets closer to the tip. It is believed that this problem can easily be solved by using larger segments and by reducing the number of measurement points. Such an approach can ensure that the laser spot will remain within the same segment during the test.

If the accuracy used in this analysis is applied to the 61.5 m long blades of the NREL 5 MW wind turbine, the corresponding spatial resolution would be 25 cm approximately. Finding the location of the damage with such a high accuracy will help the maintenance staff to detect and solve the problems more easily and efficiently.

An important issue to be considered related to the applicability of the proposed system to monitor large size structural components, such as the blades and tower of MW scale wind turbines, is the maximum measurement range of the utilized IR laser beam. Conventional IR laser vibrometers can take very accurate measurements from very long distances such as 300–400 m [31]. Since the water droplets suspended in the air act like very small size lenses and refract the laser beam, humidity is the key parameter which affects the maximum range of the measurement system. Under optimum environmental conditions (e.g., very low humidity level), the maximum range of the laser can extend up to 1000 m. However, these optimum conditions may not always be satisfied due to the challenging environmental factors encountered the field. The maximum measurement ranges reported by some laser source manufacturers (300–400 m) represent an average value which is valid for almost all weather conditions except rain and heavy fog [31].

6 Conclusions

This study aims to develop an innovative damage detection and preventive maintenance system, which can be used for continuous or periodical monitoring of wind turbine components. The main features of the proposed system, such as the measurement technique, the data analysis procedure, and the damage estimation methodology, are described in detail throughout the text.

The proposed system utilizes a ground-based IR laser scanner as the main sensor. Since conventional IR laser vibrometers cannot be used in scanning mode, a new control and guidance system is developed to be able to use these devices for scanning large objects from remote distances efficiently. The feasibility tests conducted in the laboratory clearly show that the new scanning platform allows the user to monitor and control all important measurement parameters by a computer through a user interface. A specialized software program enables complicated measurement paths or grid-like patterns to be described very easily.

Similarly, outdoor feasibility tests reveal that very complex geometries can be measured within short periods. If the same precision can be reached in scanning large structures, it is expected that the measurement points on MW scale wind turbines can be targeted with an accuracy of $\pm$ 5 cm.

Within the scope of the study, a novel and efficient damage detection algorithm is developed for the rapid analysis and

interpretation of the acquired vibration data. The applicability of the proposed methodology is demonstrated on a 61.5 m long Benchmark blade model designed for the 5 MW NREL reference wind turbine. The results of the analyses clearly show that the proposed method can estimate the location and the degree of the damage with a maximum error of 2.8%.

The developed algorithm also allows linear superposition of damage levels calculated at different segments. Therefore, it enables complicated damage scenarios involving simultaneous damage at multiple locations to be analyzed. Obtained results can be stored in a database and used to monitor the health condition of the structure regularly or after extreme events such as earthquakes or hurricanes.

The results of the outdoor vibration measurements and laboratory experiments show that the utilized methodology does not require using a FE model to determine the location of the damage. The damaged segments can always be identified very accurately by just comparing the modes of the healthy and damaged components.

The validation tests conducted in the laboratory show that the max error made in estimating the damage level is in the range of 11%. However, this value is reached for the analysis of the extreme case corresponding to approximately 70% stiffness loss. Since such a severe damage level may not be realistic, it is expected that the maximum estimation error would be in the range of 5–6% in practical applications. A major part of the observed error is considered to be related to the uncertainties in creating the physical damage on a member, not to the mathematical methodology applied. Damaging a component physically is not a fully controllable process. The acquired accuracy is considered to be very promising for implementing the proposed system for the health monitoring of large wind turbines.

The proposed damage detection system can easily be applied to existing turbines. If there are some vibration sensors, which are already installed on the turbine (accelerometers or strain gauges), they can easily be synchronized and integrated with the developed monitoring system. These systems can be used to provide the reference signal required to scale the laser measurements taken under varying excitation levels. Since the IR laser is used as a moving sensor, which scans different target points throughout the structure, the corresponding instrumentation cost is much lower compared to the conventional measurement systems. A single monitoring system can be used for the regular survey and the control of all the turbines in a wind farm. In addition, the obtained spatial resolution would absolutely be much higher. Such a high spatial resolution allows the turbine maintenance staff to detect the location of the flaws very rapidly and efficiently and take the required precautions before these flaws expand and cause irretrievable damage on the structural components.

Data Availability The data used to support the findings of this study are included within the article.

Declarations

Conflict of interest The authors declare that they have no conflict of interest.

References

1. Li, B.; Rong, K.; Cheng, H.; Wu, Y.: Fatigue assessment of monopile supported offshore wind turbine under non-Gaussian wind field. Shock Vib. 6467617 (2021)
2. Güneş, O.; Altunsu, E.; Sari, A.: Special cases in fatigue analysis of wind turbines. Wind Struct. Int. J. **32**, 501–508 (2021)
3. Yue, Y.; Tian, J.; Bai, Y.; Jia, K.; He, J.; Luo, D.; Chen, T.: Applicability analysis of inspection and monitoring technologies in wind turbine towers. Shock Vib. 5548727 (2021)
4. Xianlong, H.; Tianli, S.: A new identification method for bolt looseness in wind turbine towers. Shock Vib. 6056181 (2019)
5. Jang, Y.J.; Kim, H.J.; Kim, H.G.; Kang, K.-W.: Identification of debonding damage at spar cap-shearweb joints by artificial neural network using natural frequency relevant key features of composite wind turbine blades. Appl. Sci. **11**, 5327 (2021)
6. Nguyen, C.U.; Lee, S.Y.; Kim, H.T.; Kim, J.T.: Vibration-based damage assessment in gravity-based wind turbine tower under various waves. Shock Vib. 1406861 (2019)
7. Ricci, F.; Monaco, E.; Boffa, N.D.; Maio, L.; Memmolo, V.: Guided waves for structural health monitoring in composites: a review and implementation strategies. Prog. Aerosp. Sci. **129**, 100790 (2022)
8. Du, Y.; Zhou, S.; Jing, X.; Peng, Y.; Wu, H.; Kwok, N.: Damage detection techniques for wind turbine blades: a review. Mech. Syst. Signal Process. **141**, 106445 (2020)
9. Helming, P.; Von Freyberg, A.; Sorg, M.; Fischer, A.: Wind turbine tower deformation measurement using terrestrial laser scanning on a 3.4 MW wind turbine. Energies **14**, 1–14 (2021)
10. Zieger, T.; Nagel, S.; Lutzmann, P.; Kaufmann, I.; Ritter, J.; Ummenhofer, T.; Knodel, P.; Fischer, P.: Simultaneous identification of wind turbine vibrations by using seismic data, elastic modeling and laser Doppler vibrometry. Wind Energy **23**, 1145–1153 (2020)
11. Spanos, N.A.; Sakellariou, J.S.; Fassois, S.D.: Vibration-response-only statistical time series structural health monitoring methods: a comprehensive assessment via a scale jacket structure. Struct. Health Monit. **19**, 736–750 (2020)
12. Poozesh, P.; Baqersad, J.; Niezrecki, C.; Avitabile, P.; Harvey, E.; Yarala, R.: Large-area photogrammetry based testing of wind turbine blades. Mech. Syst. Signal Process. **86**, 98–115 (2017)

13. Poozesh, P.; Sabato, A.; Sarrafi, A.; Niezrecki, C.; Avitabile, P.; Yarala, R.: Multicamera measurement system to evaluate the dynamic response of utility-scale wind turbine blades. Wind Energy **23**, 1619–1639 (2020)
14. Dong, C.; Li, L.; Yan, J.; Zhang, Z.; Pan, H.; Catbas, F.N.: Pixel-level fatigue crack segmentation in large-scale images of steel structures using an encoder–decoder network. Sensors **21**, 1–17 (2021)
15. Dong, C.Z.; Bas, S.; Catbas, F.N.: Investigation of vibration serviceability of a footbridge using computer vision-based methods. Eng. Struct. **224**, 1–13 (2020)
16. Dong, C.Z.; Catbas, F.N.: A review of computer vision–based structural health monitoring at local and global levels. Struct. Health Monit. **20**, 692–743 (2021)
17. Srivastava, V.; Baqersad, J.: An optical-based technique to obtain operating deflection shapes of structures with complex geometries. Mech. Syst. Signal Process. **128**, 69–81 (2019)
18. Baqersad, J.; Poozesh, P.; Niezrecki, C.; Avitabile, P.: Photogrammetry and optical methods in structural dynamics: a review. Mech. Syst. Signal Process. **86**, 17–34 (2017)
19. Ozbek, M.; Rixen, D.J.: Operational modal analysis of a 2.5 MW wind turbine using optical measurement techniques and strain gauges. Wind Energy **16**, 367–381 (2013)
20. Dilek, A.U.; Oguz, A.D.; Satis, F.; Gokdel, Y.D.; Ozbek, M.: Condition monitoring of wind turbine blades and tower via an automated laser scanning system. Eng. Struct. **189**, 25–34 (2019)
21. Sahal, R.; Alsamhi, S.H.; Breslin, J.G.; Brown, K.N.; Ali, M.I.: Digital twins collaboration for automatic erratic operational data detection in industry 4.0. Appl. Sci. **11**, 3186 (2021)
22. Shittu, A.A.; Mehmanparast, A.; Hart, P.; Kolios, A.: Comparative study between S-N and fracture mechanics approach on reliability assessment of offshore wind turbine jacket foundations. Reliab. Eng. Syst. Saf. **215**, 1–15 (2021)
23. Chung, W.C.; Pestana, G.R.; Kim, M.: Structural health monitoring for TLP-FOWT (floating offshore wind turbine) tendon using sensors. Appl. Ocean Res. **113**, 1–15 (2021)
24. Bernuzzi, C.; Crespi, P.; Montuori, R.; Nastri, E.; Simoncelli, M.; Stochino, F.; Zucca, M.: Resonance of steel wind turbines: problems and solutions. Structures **32**, 65–75 (2021)
25. Castro, O.; Branner, K.: Effect of tunneling cracks on structural property degradation of wind turbine blades. Compos. Struct. **268**, 1–14 (2021)
26. Gorgin, R.; Wang, Z.: Structural damage identification based on principal curvatures of mode shape. Int. J. Acoust. Vibr. **25**, 566–576 (2021)
27. Chinka, S.S.B.; Putti, S.R.; Adavi, B.K.: Modal testing and evaluation of cracks on cantilever beam using mode shape curvatures and natural frequencies. Structures **32**, 1386–1397 (2021)
28. Meng, F.; Ozbek, M.; Rixen, D.J.; Van Tooren, M.J.L.: Comparison of system identification techniques for predicting dynamic properties of large scale wind turbines by using the simulated time response. In: Proceedings of the Society for Experimental Mechanics Series, vol. 1, pp. 339–349, Florida, USA (2011)
29. Resor, B.R.: SAND2013-2569. Definition of a 5MW/61.5m wind turbine blade reference model. Sandia National Laboratories, Albuquerque (2013)
30. PCB Piezotronics (2022). https://www.pcb.com/products?model=393B04
31. Polytec GmbH (2022). https://www.polytec.com/int